Recently Fabrizio et al. (2005) have shown that while Sir2 has a positive impact on replicative lifespan in *S. cerevisiae*, it actually has a negative impact on chronological lifespan, which is a measure of how long a non-dividing cell or organism survives. In addition, while it is generally accepted that Sirtuins positively regulate longevity in metazoans, SIRT1 may actually function in a pro-aging pathway (Fabrizio et al., 2005), as sirt1$^{-/-}$ mice manifest many phenotypes of long-lived IGF-I-deficient dwarf mice (McBurney et al., 2003). Furthermore, SIRT1 represses the DAF-16 homolog FOXO3 (Motta et al., 2004), and this is presumably antagonistic to longevity (Lin et al., 1997). If the activities of NSTs negatively regulate replicative lifespan in *N. crassa*, then competition between NSTs and NPO for NAD+ could occur, with NPO acting to promote longevity through inhibition of NSTs.

Regardless of whether Sirtuins promote or inhibit longevity, the general observation that NAD+-dependent deacetylases impact aging in both yeast and metazoans suggests conservation of this role during evolution. It is therefore reasonable to expect that NSTs may play a role in *N. crassa* as well. Until such a role has been definitively established, however, it is not possible to draw conclusions about the involvement of NSTs in the NPO pathway. Analysis of the aging phenotypes of *nst* mutants, individually and in combination with each other and the *npo* mutant, would provide an answer to these mechanistic questions.

Acknowledgments

We would like to thank Melissa Hemphill for helping to analyze *npo/nst* genetic interaction and Wendy Hanna-Rose for comments on the manuscript. Thanks to Melissa Rolls for expert advice in confocal imaging. This work was supported by grant GM025690 from the National Institutes of Health to EUS and by Rational Evolutionary Design of Advanced Biomolecules, Saitama Prefecture Collaboration of Regional Entities for the Advancement of Technological Excellence, Japan Science and Technology Agency to HI.

References

Ahel, I., Ahel, D., Matsusaka, T., Clark, A.J., Pines, J., et al., 2008. Poly(ADP-ribose)-binding zinc finger motifs in DNA repair/checkpoint proteins. Nature 451, 81–85.
Ame, J.C., Rolli, V., Schreiber, V., Niedergang, C., Apiou, F., et al., 1999. PARP-2, a novel mammalian DNA damage-dependent poly(ADP-ribose) polymerase. J. Biol. Chem. 274, 17860–17868.
Ame, J.C., Spenlehauer, C., de Murcia, G., 2004. The PARP superfamily. BioEssays 26, 882–893.
Ame, J.C., Fouquerel, E., Gauthier, L.R., Biard, D., Boussin, F.D., et al., 2009a. Radiation-induced mitotic catastrophe in PARG-deficient cells. J. Cell Sci. 122, 1990–2002.
Ame, J.C., Hakme, A., Quenet, D., Fouquerel, E., Dantzer, F., et al., 2009b. Detection of the nuclear poly(ADP-ribose)-metabolizing enzymes and activities in response to DNA damage. Method Mol. Biol. 464, 267–283.
Anderson, R.M., Bitterman, K.J., Wood, J.G., Medvedik, O., Cohen, H., et al., 2002. Manipulation of a nuclear NAD+ salvage pathway delays aging without altering steady-state NAD+ levels. J. Biol. Chem. 277, 18881–18890.
Anderson, R.M., Bitterman, K.J., Wood, J.G., Medvedik, O., Sinclair, D.A., 2003. Nicotinamide and PNC1 govern lifespan extension by calorie restriction in *Saccharomyces cerevisiae*. Nature 423, 181–185.
Aramayo, R., Metzenberg, R.L., 1996. Meiotic transvection in fungi. Cell 86, 103–113.
Barra, J.L., Rhounim, L., Rossignol, J.L., Faugeron, G., 2000. Histone H1 is dispensable for methylation-associated gene silencing in *Ascobolus immersus* and essential for long life span. Mol. Cell Biol. 20, 61–69.
Belenky, P., Bogan, K.L., Brenner, C., 2007. NAD+ metabolism in health and disease. Trends Biochem. Sci. 32, 12–19.
Beneke, S., Burkle, A., 2004. Poly(ADP-ribosyl)ation, PARP, and aging. Sci. Aging Knowledge Environ. 2004, re9.
Beneke, S., Burkle, A., 2007. Poly(ADP-ribosyl)ation in mammalian ageing. Nucleic Acids Res. 35, 7456–7465.
Bouchard, V.J., Rouleau, M., Poirier, G.G., 2003. PARP-1, a determinant of cell survival in response to DNA damage. Exp. Hematol. 31, 446–454.
Boulu, R.G., Mesenge, C., Charriaut-Marlangue, C., Verrecchia, C., Plotkine, M., 2001. Neuronal death: potential role of the nuclear enzyme, poly (ADP-ribose) polymerase. Bull. Acad. Natl. Med. 185, 555–563. discussion 564–555.
Burkle, A., 2000. Poly(ADP-ribosyl)ation: a posttranslational protein modification linked with genome protection and mammalian longevity. Biogerontology 1, 41–46.
Burkle, A., 2001a. PARP-1: a regulator of genomic stability linked with mammalian longevity. ChemBioChem 2, 725–728.
Burkle, A., 2001b. Physiology and pathophysiology of poly(ADP-ribosyl)ation. BioEssays 23, 795–806.
Burkle, A., Diefenbach, J., Brabeck, C., Beneke, S., 2005. Ageing and PARP. Pharmacol. Res. 52, 93–99.
Burzio, L.O., Riquelme, P.T., Koide, S.S., 1979. ADP ribosylation of rat liver nucleosomal core histones. J. Biol. Chem. 254, 3029–3037.
Campisi, J., 2005. Senescent cells, tumor suppression, and organismal aging: good citizens, bad neighbors. Cell 120, 513–522.
Carroll, A.M., Sweigard, J.A., Valent, B., 1994. Improved vectors for selecting resistance to hygromycin. Fungal Genet. Newsl. 41, 22.
Chiarugi, A., Moskowitz, M.A., 2002. Cell biology. PARP-1—a perpetrator of apoptotic cell death? Science 297, 200–201.
D'Amours, D., Desnoyers, S., D'Silva, I., Poirier, G.G., 1999. Poly(ADP-ribosyl)ation reactions in the regulation of nuclear functions. Biochem. J. 342 (Pt 2), 249–268.
Dantzer, F., Schreiber, V., Niedergang, C., Trucco, C., Flatter, E., et al., 1999. Involvement of poly(ADP-ribose) polymerase in base excision repair. Biochimie 81, 69–75.
Davis, R.D., DeSerres, F.J., 1970. Genetic and microbiological research techniques for *Neurospora crassa*. Methods Enzymol. 17, 79–143.
de Murcia, J.M., Niedergang, C., Trucco, C., Ricoul, M., Dutrillaux, B., et al., 1997. Requirement of poly(ADP-ribose) polymerase in recovery from DNA damage in mice and in cells. Proc. Natl. Acad. Sci. USA 94, 7303–7307.
Doucet-Chabeaud, G., Godon, C., Brutesco, C., de Murcia, G., Kazmaier, M., 2001. Ionising radiation induces the expression of PARP-1 and PARP-2 genes in Arabidopsis. Mol. Genet. Genomics 265, 954–963.
Fabrizio, P., Gattazzo, C., Battistella, L., Wei, M., Cheng, C., et al., 2005. Sir2 blocks extreme life-span extension. Cell 123, 655–667.
Folco, H.D., Freitag, M., Ramon, A., Temporini, E.D., Alvarez, M.E., et al., 2003. Histone H1 Is required for proper regulation of pyruvate decarboxylase gene expression in *Neurospora crassa*. Eukaryot Cell. 2, 341–350.
Freitag, M., Hickey, P.C., Khlafallah, T.K., Read, N.D., Selker, E.U., 2004a. HP1 is essential for DNA methylation in neurospora. Mol. Cell 13, 427–434.
Freitag, M., Hickey, P.C., Raju, N.B., Selker, E.U., Read, N.D., 2004b. GFP as a tool to analyze the organization, dynamics and function of nuclei and microtubules in *Neurospora crassa*. Fungal Genet. Biol. 41, 897–910.
Funayama, R., Saito, M., Tanobe, H., Ishikawa, F., 2006. Loss of linker histone H1 in cellular senescence. J. Cell Biol. 175, 869–880.
Gallo, C.M., Smith, D.L., Smith Jr., J.S., 2004. Nicotinamide clearance by Pnc1 directly regulates Sir2-mediated silencing and longevity. Mol. Cell Biol. 24, 1301–1312.
Grube, K., Burkle, A., 1992. Poly(ADP-ribose) polymerase activity in mononuclear leukocytes of 13 mammalian species correlates with species-specific life span. Proc. Natl. Acad. Sci. USA 89, 11759–11763.
Herceg, Z., Wang, Z.Q., 2001. Functions of poly(ADP-ribose) polymerase (PARP) in DNA repair, genomic integrity and cell death. Mutat. Res. 477, 97–110.
Honda, S., Selker, E., 2009. Tools for fungal proteomics: multifunctional neurospora vectors for gene replacement, protein expression and protein purification. Genetics.
Hong, S.J., Dawson, T.M., Dawson, V.L., 2004. Nuclear and mitochondrial conversations in cell death: PARP-1 and AIF signaling. Trends Pharmacol. Sci. 25, 259–264.
Huletsky, A., de Murcia, G., Muller, S., Hengartner, M., Menard, L., et al., 1989. The effect of poly(ADP-ribosyl)ation on native and H1-depleted chromatin. A role of poly(ADP-ribosyl)ation on core nucleosome structure. J. Biol. Chem. 264, 8878–8886.
Ikejima, M., Noguchi, S., Yamashita, R., Ogura, T., Sugimura, T., et al., 1990. The zinc fingers of human poly(ADP-ribose) polymerase are differentially required for the recognition of DNA breaks and nicks and the consequent enzyme activation. Other structures recognize intact DNA. J. Biol. Chem. 265, 21907–21913.
Jeggo, P.A., 1998. DNA repair: PARP – another guardian angel? Curr. Biol. 8, R49–R51.
Kaeberlein, M., McVey, M., Guarente, L., 1999. The SIR2/3/4 complex and SIR2 alone promote longevity in *Saccharomyces cerevisiae* by two different mechanisms. Genes Dev. 13, 2570–2580.
Karras, G.I., Kustatscher, G., Buhecha, H.R., Allen, M.D., Pugieux, C., et al., 2005. The macro domain is an ADP-ribose binding module. EMBO J. 24, 1911–1920.
Kennedy, B.K., Austriaco Jr., N.R., Zhang, J., Guarente, L., 1995. Mutation in the silencing gene SIR4 can delay aging in *S. cerevisiae*. Cell 80, 485–496.
Kim, M.Y., Mauro, S., Gevry, N., Lis, J.T., Kraus, W.L., 2004. NAD+ dependent modulation of chromatin structure and transcription by nucleosome binding properties of PARP-1. Cell 119, 803–814.
Kim, M.Y., Zhang, T., Kraus, W.L., 2005. Poly(ADP-ribosyl)ation by PARP-1: 'PAR-laying' NAD+ into a nuclear signal. Genes Dev. 19, 1951–1967.
Kouzminova, E., Selker, E.U., 2001. dim-2 encodes a DNA methyltransferase responsible for all known cytosine methylation in Neurospora. EMBO J. 20, 4309–4323.
Kraus, W.L., Lis, J.T., 2003. PARP goes transcription. Cell 113, 677–683.
Krishnakumar, R., Gamble, M.J., Frizzell, K.M., Berrocal, J.G., Kininis, M., et al., 2008. Reciprocal binding of PARP-1 and histone H1 at promoters specifies transcriptional outcomes. Science 319, 819–821.

Please cite this article in press as: Kothe, G.O., et al. PARP is involved in replicative aging in *Neurospora crassa*. Fungal Genet. Biol. (2010), doi:10.1016/j.fgb.2009.12.012

Lamming, D.W., Latorre-Esteves, M., Medvedik, O., Wong, S.N., Tsang, F.A., et al., 2005. HST2 mediates SIR2-independent life-span extension by calorie restriction. Science 309, 1861–1864.
Li, B., Navarro, S., Kasahara, N., Comai, L., 2004. Identification and biochemical characterization of a Werner's syndrome protein complex with Ku70/80 and poly(ADP-ribose) polymerase-1. J. Biol. Chem. 279, 13659–13667.
Lin, K., Dorman, J.B., Rodan, A., Kenyon, C., 1997. daf-16: an HNF-3/forkhead family member that can function to double the life-span of *Caenorhabditis elegans*. Science 278, 1319–1322.
Lin, S.J., Defossez, P.A., Guarente, L., 2000. Requirement of NAD and SIR2 for life-span extension by calorie restriction in *Saccharomyces cerevisiae*. Science 289, 2126–2128.
Lin, S.J., Ford, E., Haigis, M., Liszt, G., Guarente, L., 2004. Calorie restriction extends yeast life span by lowering the level of NADH. Genes Dev. 18, 12–16.
Loros, J.J., Denome, S.A., Dunlap, J.C., 1989. Molecular cloning of genes under control of the circadian clock in Neurospora. Science 243, 385–388.
Luo, Z., Freitag, M., Sachs, M.S., 1995. Translational regulation in response to changes in amino acid availability in *Neurospora crassa*. Mol. Cell Biol. 15, 5235–5245.
Margolin, B.S., Freitag, M., Selker, E.U., 1997. Improved plasmids for targeting at the his-3 locus of *Neurospora crassa* by electroporation. Fungal Genet. Newsl. 47, 112.
Margolin, B.S., Garrett-Engele, P.W., Stevens, J.N., Fritz, D.Y., Garrett-Engele, C., et al., 1998. A methylated Neurospora 5S rRNA pseudogene contains a transposable element inactivated by repeat-induced point mutation. Genetics 149, 1787–1797.
Masutani, M., Nakagama, H., Sugimura, T., 2003. Poly(ADP-ribose) and carcinogenesis. Genes Chromosomes Cancer 38, 339–348.
McBurney, M.W., Yang, X., Jardine, K., Hixon, M., Boekelheide, K., et al., 2003. The mammalian SIR2alpha protein has a role in embryogenesis and gametogenesis. Mol. Cell Biol. 23, 38–54.
McNally, M.T., Free, S.J., 1988. Isolation and characterization of a Neurospora glucose-repressible gene. Curr. Genet. 14, 545–551.
Meder, V.S., Boeglin, M., de Murcia, G., Schreiber, V., 2005. PARP-1 and PARP-2 interact with nucleophosmin/B23 and accumulate in transcriptionally active nucleoli. J. Cell Sci. 118, 211–222.
Menissier de Murcia, J., Ricoul, M., Tartier, L., Niedergang, C., Huber, A., et al., 2003. Functional interaction between PARP-1 and PARP-2 in chromosome stability and embryonic development in mouse. EMBO J. 22, 2255–2263.
Miao, V.P., Freitag, M., Selker, E.U., 2000. Short TpA-rich segments of the zeta-eta region induce DNA methylation in *Neurospora crassa*. J. Mol. Biol. 300, 249–273.
Michishita, E., McCord, R.A., Berber, E., Kioi, M., Padilla-Nash, H., et al., 2008. SIRT6 is a histone H3 lysine 9 deacetylase that modulates telomeric chromatin. Nature 452, 492–496.
Mortimer, R.K., Johnston, J.R., 1959. Life span of individual yeast cells. Nature 183, 1751–1752.
Mostoslavsky, R., Chua, K.F., Lombard, D.B., Pang, W.W., Fischer, M.R., et al., 2006. Genomic instability and aging-like phenotype in the absence of mammalian SIRT6. Cell 124, 315–329.
Motta, M.C., Divecha, N., Lemieux, M., Kamel, C., Chen, D., et al., 2004. Mammalian SIRT1 represses forkhead transcription factors. Cell 116, 551–563.
Ninomiya, Y., Suzuki, K., Ishii, C., Inoue, H., 2004. Highly efficient gene replacements in Neurospora strains deficient for nonhomologous end-joining. Proc. Natl. Acad. Sci. USA 101, 12248–12253.
Ogata, N., Ueda, K., Kawaichi, M., Hayaishi, O., 1981. Poly(ADP-ribose) synthetase, a main acceptor of poly(ADP-ribose) in isolated nuclei. J. Biol. Chem., 4135–4137.
Osiewacz, H.D., 2002. Aging in fungi: role of mitochondria in Podospora anserina. Mech. Ageing Dev. 123, 755–764.
Panzeter, P.L., Althaus, F.R., 1990. High resolution size analysis of ADP-ribose polymers using modified DNA sequencing gels. Nucleic Acids Res. 18, 2194.
Pieper, A.A., Verma, A., Zhang, J., Snyder, S.H., 1999. Poly(ADP-ribose) polymerase, nitric oxide and cell death. Trends Pharmacol. Sci. 20, 171–181.
Povirk, L.F., Wubter, W., Kohnlein, W., Hutchinson, F., 1977. DNA double-strand breaks and alkali-labile bonds produced by bleomycin. Nucleic Acids Res. 4, 3573–3580.
Reale, A., Matteis, G.D., Galleazzi, G., Zampieri, M., Caiafa, P., 2005. Modulation of DNMT1 activity by ADP-ribose polymers. Oncogene 24, 13–19.
Riquelme, P.T., Burzio, L.O., Koide, S.S., 1979. ADP ribosylation of rat liver lysine-rich histone in vitro. J. Biol. Chem. 254, 3018–3028.
Rogina, B., Helfand, S.L., 2004. Sir2 mediates longevity in the fly through a pathway related to calorie restriction. Proc. Natl. Acad. Sci. USA 101, 15998–16003.
Rountree, M.R., Selker, E.U., 1997. DNA methylation inhibits elongation but not initiation of transcription in *Neurospora crassa*. Genes Dev. 11, 2383–2395.
Sandmeier, J.J., Celic, I., Boeke, J.D., Smith, J.S., 2002. Telomeric and rDNA silencing in *Saccharomyces cerevisiae* are dependent on a nuclear NAD(+) salvage pathway. Genetics 160, 877–889.
Selker, E.U., 1990. Premeiotic instability of repeated sequences in *Neurospora crassa*. Annu. Rev. Genet. 24, 579–613.
Selker, E.U., 2004. Genome defense and DNA methylation in Neurospora. Cold Spring Harb. Symp. Quant. Biol. 69, 119–124.
Selker, E.U., Fritz, D.Y., Singer, M.J., 1993. Dense nonsymmetrical DNA methylation resulting from repeat-induced point mutation in Neurospora. Science 262, 1724–1728.
Selker, E.U., Tountas, N.A., Cross, S.H., Margolin, B.S., Murphy, J.G., et al., 2003. The methylated component of the *Neurospora crassa* genome. Nature 422, 893–897.
Semighini, C.P., Savoldi, M., Goldman, G.H., Harris, S.D., 2006. Functional characterization of the putative *Aspergillus nidulans* poly(ADP-ribose) polymerase homolog PrpA. Genetics 173, 87–98.
Shieh, W.M., Ame, J.C., Wilson, M.V., Wang, Z.Q., Koh, D.W., et al., 1998. Poly(ADP-ribose) polymerase null mouse cells synthesize ADP-ribose polymers. J. Biol. Chem. 273, 30069–30072.
Shimokawa, T., Masutani, M., Nagasawa, S., Nozaki, T., Ikota, N., et al., 1999. Isolation and cloning of rat poly(ADP-ribose) glycohydrolase: presence of a potential nuclear export signal conserved in mammalian orthologs. J. Biochem. 126, 748–755.
Shiu, P.K., Raju, N.B., Zickler, D., Metzenberg, R.L., 2001. Meiotic silencing by unpaired DNA. Cell 107, 905–916.
Sinclair, D.A., Guarente, L., 1997. Extrachromosomal rDNA circles—a cause of aging in yeast. Cell 91, 1033–1042.
Smith, K.M., Kothe, G.O., Matsen, C.B., Khlafallah, T.K., Adhvaryu, K.K., et al., 2008. The fungus *Neurospora crassa* displays telomeric silencing mediated by multiple sirtuins and by methylation of histone H3 lysine 9. Epigenet. Chromatin 1.
Smulson, M.E., Simbulan-Rosenthal, C.M., Boulares, A.H., Yakovlev, A., Stoica, B., et al., 2000. Roles of poly(ADP-ribosyl)ation and PARP in apoptosis, DNA repair, genomic stability and functions of p53 and E2F-1. Adv. Enzyme Regul. 40, 183–215.
Tamaru, H., Selker, E.U., 2001. A histone H3 methyltransferase controls DNA methylation in *Neurospora crassa*. Nature 414, 277–283.
Tissenbaum, H.A., Guarente, L., 2001. Increased dosage of a sir-2 gene extends lifespan in *Caenorhabditis elegans*. Nature 410, 227–230.
Trucco, C., Oliver, F.J., de Murcia, G., Menissier-de Murcia, J., 1998. DNA repair defect in poly(ADP-ribose) polymerase-deficient cell lines. Nucleic Acids Res. 26, 2644–2649.
Tsuchiya, M., Dang, N., Kerr, E.O., Hu, D., Steffen, K.K., et al., 2006. Sirtuin-independent effects of nicotinamide on lifespan extension from calorie restriction in yeast. Aging Cell 5, 505–514.
Tulin, A., Stewart, D., Spradling, A.C., 2002. The Drosophila heterochromatic gene encoding poly(ADP-ribose) polymerase (PARP) is required to modulate chromatin structure during development. Genes Dev. 16, 2108–2119.
Verdun, R.E., Karlseder, J., 2007. Replication and protection of telomeres. Nature 447, 924–931.
von Kobbe, C., Harrigan, J.A., Schreiber, V., Stiegler, P., Piotrowski, J., et al., 2004. Poly(ADP-ribose) polymerase 1 regulates both the exonuclease and helicase activities of the Werner syndrome protein. Nucleic Acids Res. 32, 4003–4014.
Wang, Z.Q., Auer, B., Stingl, L., Berghammer, H., Haidacher, D., et al., 1995. Mice lacking ADPRT and poly(ADP-ribosyl)ation develop normally but are susceptible to skin disease. Genes Dev. 9, 509–520.
Wang, Z.Q., Stingl, L., Morrison, C., Jantsch, M., Los, M., et al., 1997. PARP is important for genomic stability but dispensable in apoptosis. Genes Dev. 11, 2347–2358.
Watanabe, K., Sakuraba, Y., Inoue, H., 1997. Genetic and molecular characterization of *Neurospora crassa* mus-23: a gene involved in recombinational repair. Mol. Gen. Genet. 256, 436–445.
Watanabe, F., Fukazawa, H., Masutani, M., Suzuki, H., Teraoka, H., et al., 2004. Poly(ADP-ribose) polymerase-1 inhibits ATM kinase activity in DNA damage response. Biochem. Biophys. Res. Commun. 319, 596–602.
Zong, W.X., Ditsworth, D., Bauer, D.E., Wang, Z.Q., Thompson, C.B., 2004. Alkylating DNA damage stimulates a regulated form of necrotic cell death. Genes Dev. 18, 1272–1282.

Please cite this article in press as: Kothe, G.O., et al. PARP is involved in replicative aging in *Neurospora crassa*. Fungal Genet. Biol. (2010), doi:10.1016/j.fgb.2009.12.012

平成19年度～21年度 厚生労働科学研究費補助金
第3次対がん総合戦略研究事業 中釜班
総合研究報告書 2／3冊

疾患モデル動物を用いた環境発がんの初期発生過程及び感受性要因の解明とその臨床応用に関する研究

中釜 斉

Physiol Genomics 32: 335–342, 2008.
First published November 27, 2007; doi:10.1152/physiolgenomics.00158.2007.

Evaluation of LEXF/FXLE rat recombinant inbred strains for genetic dissection of complex traits

Birger Voigt,[1] Takashi Kuramoto,[1] Tomoji Mashimo,[1] Toshiko Tsurumi,[1] Yoshiyuki Sasaki,[2] Ryoji Hokao,[2] and Tadao Serikawa[1]

[1]*Institute of Laboratory Animals, Graduate School of Medicine, Kyoto University, Sakyo-ku, Kyoto; and* [2]*Institute for Animal Reproduction, Fukaya, Kasumigaura, Ibaraki, Japan*

Submitted 15 July 2007; accepted in final form 22 November 2007

Voigt B, Kuramoto T, Mashimo T, Tsurumi T, Sasaki Y, Hokao R, Serikawa T. Evaluation of LEXF/FXLE rat recombinant inbred strains for genetic dissection of complex traits. *Physiol Genomics* 32: 335–342, 2008. First published November 27, 2007; doi:10.1152/physiolgenomics.00158.2007.—Recombinant inbred (RI) strains are formed from an outcross between two well-characterized inbred stains followed by at least 20 generations of inbreeding. RI strains can be utilized for the analysis of many complex phenotypic traits. The LEXF/FXLE RI strain set consists of 34 RI strains derived by reciprocal crossing of LE/Stm and F344/Stm. Here we report on genetic dissections of complex traits using this RI set and their parental strains. We have developed strain distribution patterns for 232 informative simple sequence length polymorphism markers. The framework map covers the rat genome except for chromosome Y. Seventy-six phenotype parameters, which included physiological and behavioral traits, were examined for these RI lines. Quantitative trait locus (QTL) analysis of these parameters revealed 27 significant and 91 suggestive QTLs, illustrating the potential of this RI resource for the detection of underlying gene functions for various phenotypes. Although this RI set was originally developed to study susceptibility to chemical-induced tumors, it has been shown to be equally powerful for a wide spectrum of traits. The LEXF/FXLE RI strains have been deposited at the National Bio Resource Project for the Rat in Japan and are maintained under specific pathogen-free conditions. They are available at **http://www.anim.med.kyoto-u.ac.jp/nbr**.

Rattus norvegicus; recombinant inbred rats; quantitative trait locus mapping; physiological traits

THE DISCOVERY OF GENE FUNCTIONS related to human diseases is still a major issue in biomedical research. A large number of single genes have already been identified as underlying modifications associated with various monogenic disorders. Moreover, numerous articles on the dysfunctions of single gene defects exist, but the consequences of allelic variations on the complex physiological network as well as the various players of this network remain largely unknown. The NCBI database Online Mendelian Inheritance in Man contains 17,744 entries, of which only 386 are on genes with known sequences and phenotypes (14). Since all complex phenotypes result from interactions between numerous genes, quantitative trait locus (QTL) analysis in rodent models is an important method for unraveling these phenotypes and extrapolating the results to human studies. The number of such QTL experiments that have already been performed is enormous. To date, 3,538 QTLs are described in the Mouse Genome Database (16) and 1,302 QTLs are listed in the Rat Genome Database (19). Even though the majority of the listed QTLs were obtained from F2 or backcross studies, one could be misled to underestimate the role of recombinant inbred (RI) lines since they have been utilized in rodents for more than 40 years (3, 4, 7, 15, 25). However, the majority of the RI lines originated from mouse strains, and only a few rat-derived RI lines are or were available (1, 8, 18, 20, 23).

Successful QTL mapping always depends on diverse phenotypes and genotypes and a statistical method for determining the odds between phenotype and genotype patterns. This diversification of phenotypes combined with numerous recombination events across the rat genome are given requirements for the largest RI rat strain set available, the LEXF/FXLE strains, which were historically generated to study genes involved in tumor genesis. Considering the QTLs that have already been described in other experiments (19) and the theoretical power of the LEXF/FXLE strains, the questions that we wanted to answer in this study cover two aspects: *1*) the scientific value of this RI panel as a tool for the dissection of quantitative traits and *2*) the number and nature of the detected QTLs themselves. In other words, we asked whether or not these RI strains can be utilized for the determination of QTLs for physiological and other randomly analyzed phenotypic parameters despite the LEXF/FXLE's initial research purpose being only based on their different susceptibility to chemical-induced tumors. Furthermore, if QTLs are detectable, we wanted to know how effective this set of RI strains is for identifying QTLs for randomly examined phenotypic parameters. Finally, we examined whether the QTLs that are obtained are new compared with previously known QTLs or whether they confirm independently computed results from other experiments. For instances where these questions can be definitively answered, the LEXF/FXLE panel could become a universal tool for the detection of virtually every type of physiological QTL.

MATERIALS AND METHODS

Animals. The LEXF/FXLE RI strains and their parental strains, F344/Stm and LE/Stm, were originally generated at the Saitama Cancer Center Research Institute by Shisa et al. (20). LE/Stm was derived from a closed Long-Evans colony from the Ben May Laboratory for Cancer Research of the University of Chicago, and F344/Stm originated from F344/DuCrj (Charles River Japan). The strains were inbred at the Saitama Institute for more than 50 and 23 generations, respectively. The RI lines were generated in two phases: first the LEXF strains were established, followed by the FXLE strains. Several RI lines had substrains that branched out at the 7th to 11th

Article published online before print. See web site for date of publication (http://physiolgenomics.physiology.org).

Address for reprint requests and other correspondence: T. Serikawa, Inst. of Laboratory Animals, Graduate School of Medicine, Kyoto Univ., Yoshidakonoe-cho, Sakyo-ku, Kyoto 606-8501, Japan (e-mail: serikawa@anim.med.kyoto-u.ac.jp).

generation after an attempt to fix the coat color. These sublines are indicated by the letters B–D following the strain number, e.g., LEXF8D. Further details on the history of these RI strains are described elsewhere (20, 23). The following strains were used for this study, with the inbred generations indicated in parentheses: F344/Stm (F69), LE/Stm (F95), LEXF1A (F51), LEXF1C (F48), LEXF2A (F50), LEXF2B (F54), LEXF2C (F54), LEXF3 (F52), LEXF4 (F50), LEXF5 (F52), LEXF6B (F46), LEXF7A (F51), LEXF7B (F53), LEXF7C (F49), LEXF8A (F51), LEXF8D (F50), LEXF9 (F53), LEXF10A (F54), LEXF10B (F49), LEXF10C (F54), LEXF11 (F53), FXLE12 (F27), FXLE13 (F27), FXLE14 (F26), FXLE15 (F30), FXLE16 (F26), FXLE17 (F25), FXLE18 (F26), FXLE19 (F28), FXLE20 (F27), FXLE21 (F28), FXLE22 (F30), FXLE24 (F24), FXLE25 (F28), and FXLE26 (F26). Since the genotyping performed in this study revealed breeding contamination for the FXLE23 strain, only 33 of 34 RI lines were analyzed. Since the rederivation of FXLE23 from uncontaminated embryos has almost been accomplished, it will be possible for future experiments to be carried out with all 34 RI strains. The rats were maintained at the specific pathogen-free facility of the Institute for Animal Reproduction. At 5 wk of age, six male rats from each strain were shipped to the Environmental Biological Life Science Research Center for phenotype screening. All animals were maintained under a 12:12-h light-dark cycle with lights on at 7:00 AM and ambient conditions of 23 ± 3°C and 55 ± 15% humidity. They were housed in groups of three animals per

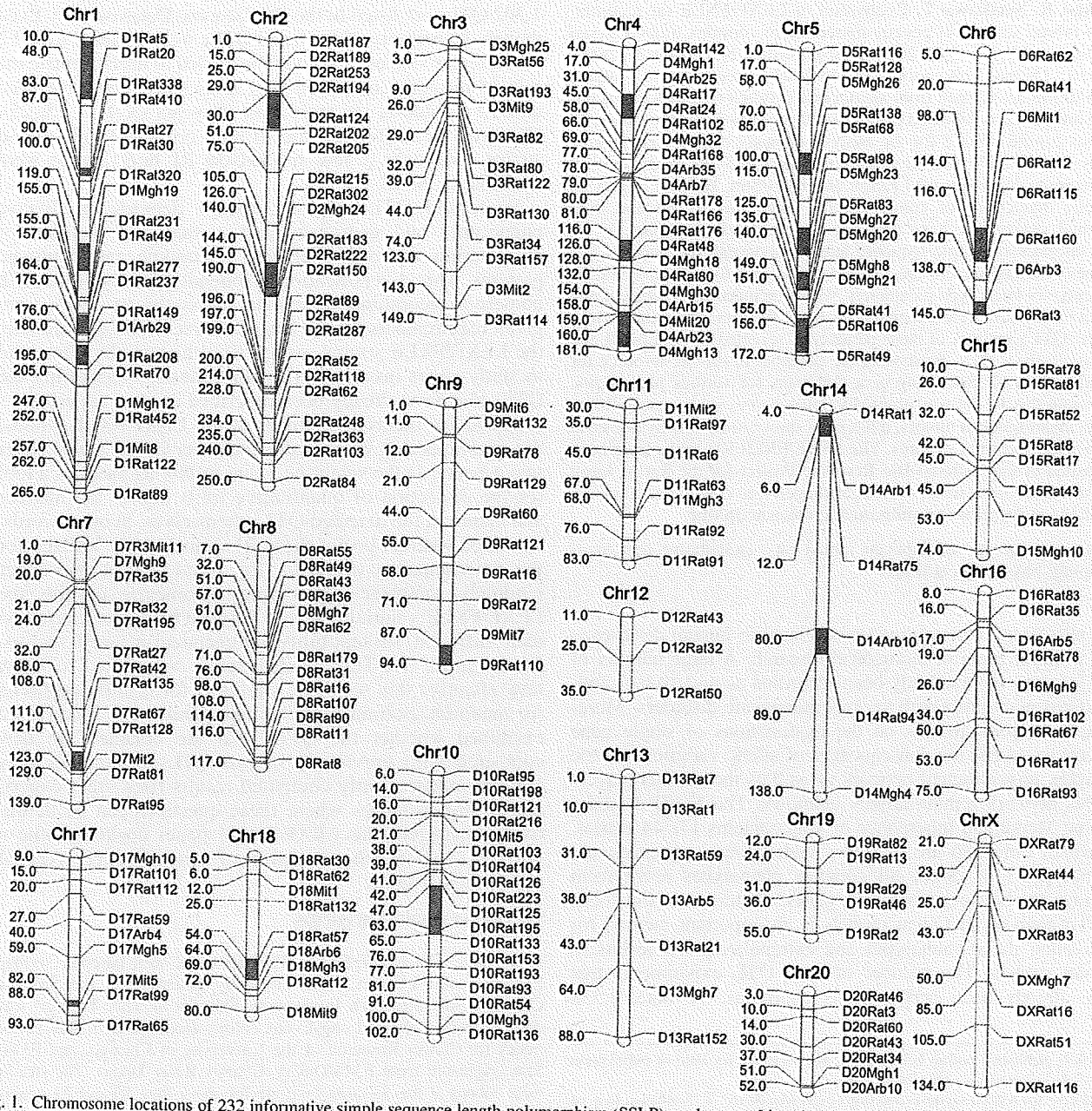

Fig. 1. Chromosome locations of 232 informative simple sequence length polymorphism (SSLP) markers used in this study. Scale roughly corresponds to their physical locations in Mbp. Gray areas indicate the positions of significant quantitative trait loci (QTLs). Suggestive QTLs are not shown for the sake of clarity. Detailed information on all QTLs is available from Table 1 and also online at **http://www.anim.med.kyoto-u.ac.jp/NBR/RI_SSLP_QTLs/SSLP_QTLs.htm**.

aluminum cage (dimensions of 240 × 380 × 200 mm) and were given free access to acidified water and chow (CE2, CLEA). Animal care and all experimental procedures were approved by the Animal Research Committee, Graduate School of Medicine, Kyoto University (approved no. MedKyo07001).

Phenotyping. Phenotypic profiles for this project consisted of the following 7 categories covering 109 parameters: *1*) functional observational battery (FOB, neurobehavioral test), *2*) behavior studies, *3*) blood pressure, *4*) urine parameters, *5*) biochemical blood tests, *6*) hematology, and *7*) anatomy (see Table 2). All measurements were performed on all male rats from each strain from 5 to 10 wk of age. The detailed protocols used for measurements of these parameters are available on our website at **http://www.anim.med.kyoto-u.ac.jp/nbr/phenotype** and were described previously (13). QTL analysis was performed with a subset of 76 quantitative parameters, which were part of the above-mentioned phenotypic profiles.

Genotyping. The genetic profiles consisted of 357 simple sequence length polymorphism (SSLP) markers with known genomic locations, which are distributed throughout the rat chromosomes except for chromosome Y. Detailed marker information is available at the National Bio Resource Project (NBRP) home page at **http://www.anim.med.kyoto-u.ac.jp/NBR/Genotyping.htm**. Genomic DNA was extracted from the spleen. The product sizes of the SSLP markers were determined with an ABI3100 DNA sequencer (Applied Biosystems).

The phylogenetic tree of the RI strains was obtained through maximum parsimony analysis implemented in PAUP 4.0b10 (22) on the basis of 259 markers that were polymorphic between the parental strains. An initial heuristic search using Fitch parsimony was carried out with 1,000 random addition sequence replicates, followed by a tree bisection-reconnection (TBR) branch swapping algorithm. Tree stability was estimated by bootstrap analysis on 1,000 replicates where the characteristics were sampled with equal probability. TreeView (**http://taxonomy.zoology.gla.ac.uk/rod/treeview.html**) was used to display the resulting tree (17).

QTL analysis. Two hundred thirty-two markers of 357 tested were informative for the RI strains and were therefore included in the genetic map for subsequent QTL scans. The basis for marker positioning and order, however, was not recombination fractions but their known location on the physical map. Genomewide scans for QTLs were performed with the 76 mean and variance values from 35 strains and the physical map of 232 genetic markers noted above. Calculations were performed with MapManager QTXb20, which is available at **http://www.mapmanager.org/** (12). Interval mapping was performed by fitting a regression equation along the genetic map to a hypothetical QTL in 1-cM steps with an additive regression model. Permutation tests were performed to empirically determine the significance thresholds for all QTL mapping results. A minimum of 1,000 permutations for each QTL calculation for the constrained additive regression model were applied to establish individual suggestive, significant, and highly significant thresholds, which correspond to genomewide probabilities for the 37th, 95th, and 99.9th percentiles, respectively, as proposed by Lander and Kruglyak (11).

RESULTS

Genetic features. Two hundred fifty-nine of 357 markers that were tested were polymorphic between the parental strains LE/Stm and F344/Stm. Twenty-seven of these polymorphic markers did not show recombination with neighboring markers among any RI strains and were therefore not included in the physical map; hence, 232 markers were informative and were utilized for QTL calculations (Fig. 1). The markers comprised in total ~2.4 Gbp on the physical map, which is ~90% of the rat genome (6). The SSLP markers provided in total 2,821 recombinations in these 33 RI strains and showed an average spacing of ~12 Mbp (Table 1), with the largest gap being 78 Mbp on chromosome 6.

The genetic relationship among the RI and parental strains on the basis of the utilized SSLP markers is displayed in Fig. 2, which reflects their historical breeding processes and substrains as previously described (20, 23).

QTL mapping efficiency of this RI panel. Analysis of the phenotypic parameters revealed that 43 of 76 mean values were significantly different between the parental F344/Stm and LE/Stm strains (Table 2). In total, 118 QTLs were detected by interval mapping, of which 27 passed the significant or highly significant criteria and 91 showed suggestive linkages (Table 2). Twenty-two traits (28%) could not be associated with any QTL. Thirty-five QTLs (30%) were associated with 20 traits (26%) that did not show significant phenotypic differences between the parental strains as indicated in Table 2. One hundred two QTLs were to our knowledge new and not described in the RGD QTL database (19). Sixteen were confirmed by this database, of which 11 and 5 were suggestive and significant, respectively. Figure 3 shows six representative highly significant QTLs that were found in this study. Further details on all QTLs detected can be obtained from Table 2 or online at **http://www.anim.med.kyoto-u.ac.jp/NBR/RI_SSLP_QTLs/SSLP_QTLs.htm**.

Table 1. *Statistics on SSLP markers and QTLs*

Chromosome	Recombinations	Mbp Covered	Average Spacing, Mbp	Recombinations per Mbp	QTLs
1	342	255	13	1.34	13
2	220	249	11	0.88	16
3	135	148	13	0.91	4
4	244	177	9	1.38	7
5	196	171	12	1.15	9
6	184	140	20	1.31	5
7	128	138	11	0.93	1
8	172	110	9	1.56	2
9	120	93	10	1.29	4
10	126	96	6	1.31	13
11	77	53	9	1.45	6
12	40	24	12	1.67	4
13	62	87	15	0.71	3
14	84	134	26	0.63	7
15	106	64	9	1.66	0
16	90	67	8	1.34	3
17	117	84	10	1.39	4
18	122	75	9	1.63	6
19	56	93	11	0.60	3
20	84	49	8	1.71	4
X	116	113	16	1.03	4
Total	2,821	2,420	11.8	1.23	118

Recombinations, no. of recombination events on each chromosome that occurred during the breeding of the recombinant inbred (RI) strains and are now manifested for these RI lines on the basis of the 232 informative simple sequence length polymorphism (SSLP) markers. Mbp covered, genomic region that is covered by the SSLP for each chromosome (in Mbp) and is calculated from the physical position of the markers. Average spacing of the markers and recombinations per Mbp are computed from the no. of recombinations and Mbp covered and refer to the marker numbers. Quantitative trait loci (QTLs) detected for each chromosome include suggestive, significant, and highly significant QTLs. Note: Although there is a strong correlation between Mbp covered and QTLs, no correlation could be found between recombinations per Mbp and QTLs (data not shown).

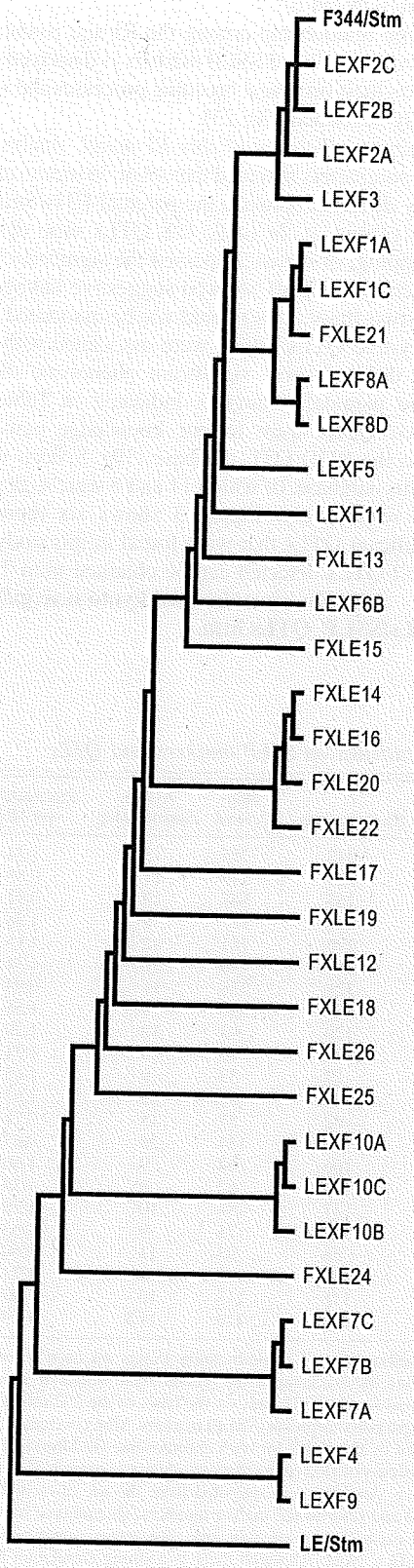

Fig. 2. Genetic relationship between recombinant inbred (RI) and parental strains on the basis of 259 polymorphic SSLP markers. Note: since laboratory rat strains in general and RI strains in particular do not refer to different species as usually indicated in phylogenetic trees, this figure should be interpreted as an overview of how far or how close each RI line is related to other RI and parental strains if it is assumed that the relationship computation is started from LE/Stm.

DISCUSSION

The initial screening for QTLs using 232 informative SSLP markers in these 33 LEXF/FXLE RI and 2 parental strains already revealed 118 QTLs for 54 quantitative parameters, which is equivalent to a rate of ~70% when referring to the 76 parameters examined. These pure numbers indicate that this RI panel is a powerful tool for QTL mapping and shows promise for use in further dissections of quantitative traits. It can be concluded by simple statistics that a QTL can be detected for two of three randomly examined parameters. However, a closer look shows that the strength of the obtained QTL seems to depend on the different natures of the parameters that were examined. All analyzed quantitative parameters are likely to be controlled by more than one gene, and it is thought that the strength of a QTL is higher when fewer genes contribute to it. In other words, the detection of a QTL becomes more difficult if many genes account for the phenotypic variance with a relatively similar, low size. This observation can also be seen in our data. The parameters that were examined can be roughly divided into two groups: simple physiological parameters such as organ weights, enzyme activities, or ion concentrations and more complex behavioral traits like rearing, locomotor activity, or passive avoidance tests. Many high-score likelihood ratio statistics (LRS) values were calculated for physiological parameters, but the LRS levels for all behavioral parameters were always only in the range of the empirically calculated suggestive threshold, confirming the complex characters of these traits. The difficulties in detecting weak QTLs are not only relevant for studies that utilize standard sib-mated RI strains. Valdar et al. (24) simulated a QTL analysis on a basis of 1,000 individuals for several breeding strategies, including normal F2 intercross, backcross, advanced intercross RI lines, heterogeneous stock RI lines, and various forms of collaborative cross approaches. They showed that a simple mapping computation based on a single marker regression model can guarantee the detection only of QTLs with effect sizes of 30% or greater. QTLs with smaller effects can be detected, but they may be overlooked. A more sophisticated mapping calculation such as composite interval mapping may lower this threshold to 10% of the trait variance, provided that 1,000 individuals are utilized in various breeding strategies (24).

To date, QTL studies mostly utilize F2 or backcross animals to map loci related to a specific phenotype for which the parental strains show highly significant differences and therefore highly segregating QTLs. Such crosses are time- and resource intensive but have the advantage that they can be used to produce maps down to the resolution of single genes. This is especially successful in the case of virtual monogenic QTLs (2, 5). In contrast, the benefit of RI strains is the fast experimental approach since the use of RI strains avoids long-term crossing periods as well as genotyping and provides ad hoc a sufficient number of recombination events. This makes it possible to reduce the experimental effort for QTL mapping using RI

Table 2. *QTL summary*

Trait	Suggestive QTL, chromosome(LRS)	Significant QTL, chromosome(LRS)	Highly Significant QTL, chromosome(LRS)	Phenotype Parental
Body wt 5 wk				ns
Body wt 6 wk				*
Body wt 10 wk	2 (10.8)			†
Brain wt 10 wk	3 (11.0)			†
Heart wt 10 wk				†
Lung wt 10 wk		14 (16.0)		ns
Liver wt 10 wk	2 (8.2)			†
Kidney wt 10 wk				†
Spleen wt 10 wk				†
Adrenals wt 10 wk	11 (9.0), 18 (11.8)			†
Testis wt 10 wk	11 (8.5), 20 (9.1)	6 (17.7)		ns
Relative brain wt 10 wk	2 (9.7)			*
Relative heart wt 10 wk	10 (8.2), 13 (9.0)			ns
Relative lung wt 10 wk		10 (18.3)		†
Relative liver wt 10 wk	5 (8.7), 16 (12.3)	18 (16.3)		†
Relative kidney wt 10 wk	2 (11.9), 11 (11.4), 12 (9.4)			ns
Relative spleen wt 10 wk	1 (13.7), 12 (11.4)			†
Relative adrenals wt 10 wk	18 (10.7)	7 (14.8)		ns
Relative testis wt 10 wk	5 (12.9), 6 (13.1)	2 (17.2)		†
Systolic blood pressure	10 (12.5), 17 (11.9)			ns
Heart rate	11 (9.2), 20 (8.2)	2 (24.5)	14 (35.0)	†
Body temperature	10 (14.5)			*
Red blood cell number	10 (8.9), 11 (10.2), X (8.1)			ns
Hemoglobin concentration	10 (9.5)			ns
Hematocrit	1 (11.3), 1 (14.0), X (13.4)	1 (15.8)		†
Mean corpuscular volume		1 (15.5)		†
Mean cell hemoglobin mass				ns
Mean cell hemoglobin concentration	1 (13.9), 1 (11.6), 1 (12.3)		1 (19.1)	†
White blood cell number				ns
Platelet number	9 (13.5), 17 (13.3)			†
Prothrombin time		14 (15.1)		ns
Activated partial thromboplastin time				†
Glutamate oxalacetate transaminase	X (8.0)			ns
Glutamate pyruvate transaminase	2 (12.4), 12 (8.4)	4 (19.4)		ns
Alkaline phosphatase	1 (15.1), 10 (11.3), 17 (11.1), 19 (10.5)		5 (46.1)	†
Total protein	10 (10.5), 19 (15.2)	17 (18.1)		†
Albumin	8 (10.4)			ns
Albumin total protein ratio	2 (13.5), X (10.1)			†
Glucose	1 (8.0), 2 (10.7), 13 (9.6)			†
Total cholesterol	3 (8.8), 10 (11.6), 16 (14.2)	5 (17.3), 18 (22.4)	5 (21.8)	†
High-density lipoprotein	3 (9.5), 4 (12.0), 5 (14.1), 10 (10.4), 16 (14.2)		5 (22.5), 18 (26.7)	†
Low-density lipoprotein	5 (9.7), 14 (13.1), 18 (13.9)	10 (20.6)		*
Triglyceride	2 (10.5), 9 (10.4), 13 (14.0)	2 (17.3)		†
Total bilirubin	1 (11.1)			†
Blood urea nitrogen	9 (9.4), 14 (11.8)			†
Creatinine	11 (12.1)			ns
Inorganic phosphate				ns
Calcium (plasma)	2 (8.4), 19 (10.9)			†
Sodium (plasma)				ns
Potassium (plasma)				ns
Chloride (plasma)				†
White blood cells				
Basophils				ns
Eosinophils	14 (14.7)	6 (16.5)		†
Stab form leukocytes				ns
Segmented leukocytes				*
Lymphocytes				ns
Monocytes	14 (10.3)			ns
Other				ns
Urine volume	2 (9.9)			ns
Sodium (urine)	10 (9.8)	1 (15.2), 9 (15.9)		†
Potassium (urine)	2 (9.4), 4 (8.5), 8 (8.8)	4 (16.9)		ns
Chloride (urine)				ns
Relative urine volume				ns
Relative sodium concentration (urine)		4 (15.9)		ns
Relative potassium concentration (urine)	2 (13.6)			†
Relative chloride concentration (urine)	4 (10.3)			ns
Rearings				†

Continued

Table 2.—*Continued*

Trait	Suggestive QTL, chromosome(LRS)	Significant QTL, chromosome(LRS)	Highly Significant QTL, chromosome(LRS)	Phenotype Parental
Forelimb grip strength	6 (13.5)			‡
Hindlimb grip strength	3 (13.8)			*
Landing foot splay	2 (9.5), 5 (8.6), 6 (9.1)			‡
Locomotor activity				
10 min				
20 min				ns
30 min	20 (11.3)			*
Total	4 (9.1)			†
Passive avoidance test training time	20 (9.9)			†
Passive avoidance test retention time	10 (11.4), 12 (9.4)			ns
				ns

QTLs are divided according to the calculation software MapManager into the categories of suggestive, significant, and highly significant. These thresholds were established empirically by 1,000 permutations for each trait. The chromosome location and likelihood ratio statistic value (LRS) are shown. The LOD score can be calculated by dividing the LRS by 4.6. Phenotype parental describes statistical differences for each phenotype parameter between the parental F344/Stm and LE/Stm calculated with the 2-tailed, unpaired *t*-test. *P 0.01–0.05, †P 0.001–0.01, ‡$P < 0.001$; ns, $P > 0.05$.

strains to only the phenotyping. However, this advantage is also a limiting factor in terms of the analytical power of RI strains. Single genes have to our knowledge not yet been mapped in QTL experiments using RI panels. More than 500 sophisticated bred RI lines would be required to detect weak QTLs that account for 5% of the phenotypic variation to within <1 cM (24). This is far more accurate than the resolution of the QTLs obtained in this study. Their confidence intervals are in most cases larger than 20 Mbp, which corresponds to several hundred candidate genes. Logical subtraction can be used to exclude most of them, but too many putative candidate genes remain to allow successful causative gene detection. Nonetheless there remains the potential to increase the accuracy of this RI resource by increasing the density of the markers. This study describes the results of QTL mapping using only 232 SSLP markers, which leaves several huge gaps of >50 Mbp in the rat genome. Currently, the STAR consortium (21) is determining the sequence for up to 100,000 single nucleotide polymorphism (SNP) loci for many rat strains, including those in this resource, and it is expected to generate a SNP map for these RI strains that will consist of ~30,000 SNPs (Hübner N, personal communication). Not all of these will be informative because of the limited number of recombinations among these 34 RI lines, but it can be assumed that these SNPs will greatly increase the accuracy of QTL mapping using this RI panel. Another way to increase the number and probably also the accuracy for the QTLs for this RI panel is the application of different and more sophisticated calculation methods. Standard interval mapping as used here takes into account only single markers, whereas in contrast composite interval mapping also takes the effect of other loci into account. Such calculations have not been performed yet because the primary goal of this study was the general evaluation of this RI panel for QTL mapping and because the upcoming SNP map will allow for a more detailed dissection of these complex traits. This is also the reason why we are not dissecting every QTL that we obtain

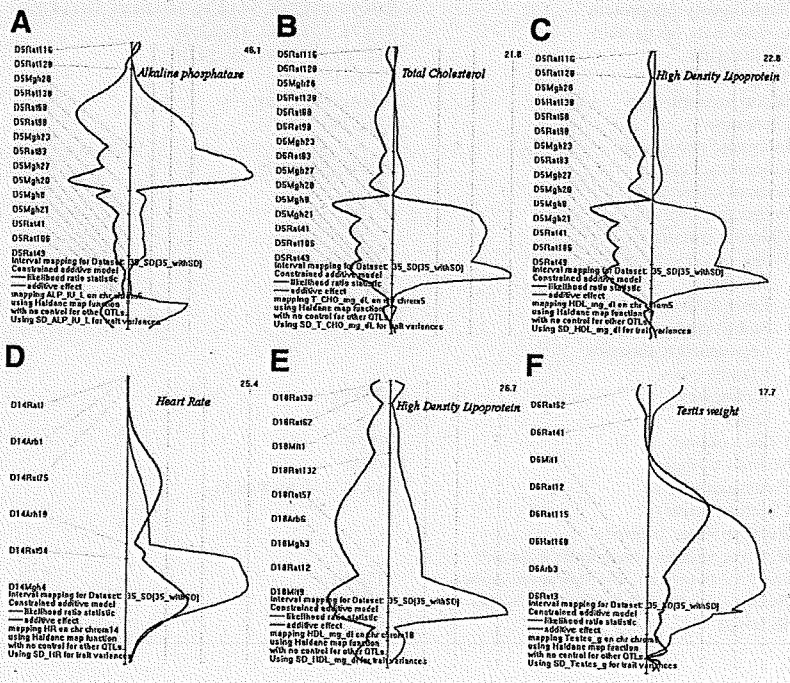

Fig. 3. Highly significant QTLs obtained from interval mapping. The black lines indicate the likelihood ratio statistics (LRS) values; the red lines illustrate the additive effect. If a red line is positive, it can be assumed that LE/Stm alleles increase the parameter. A negative red line indicates that F344/Stm increases the parameter in question. The 3 green vertical lines in each chart denote the suggestive, significant, and highly significant thresholds. *A*: QTLs for alkaline phosphatase on chromosome 5. *B*: QTLs for total cholesterol on chromosome 5. *C*: QTLs for high-density lipoprotein on chromosome 5. *D*: QTLs for heart rate on chromosome 14. *E*: QTLs for high-density lipoprotein on chromosome 18. *F*: QTLs for testis weight on chromosome 6.

and are publishing them without further discussion regarding candidate genes or cross-species comparison. Their value might seem limited because of the relatively rough genome-wide 232-marker map, but their correctness—not accuracy—should not be underestimated. The result that in total 102 of 118 QTLs are not contained in the RGD QTL database (19) is due to the majority of these parameters never having been examined in QTL research in the rat before. On the other hand, QTLs for common parameters such as cholesterol, glucose concentration, or heart weight were confirmed by our results, which was also the reason why we decided to publish not only significant but also suggestive QTLs. They confirm the results of other independent experiments and prove the investigative power of the LEXF/FXLE RI strains.

Another interesting finding of this work is the subset of the 20 detected QTLs for which the parameters of the parental strains F344/Stm and LE/Stm are not significantly different. Standard trait dissection in RI strains starts with phenotypic examination of the trait in the parental strains. If the parental strains show distinct values for the parameter it can be assumed that the corresponding genes will segregate among the RI progeny along with the QTLs, which can then easily be detected. This raises the question of how it is possible to find QTLs if the parental strains do not show significant differences for a particular trait. The answer to this lies in the complex regulation of the 20 traits, which show a wide range of phenotypic values among the RI strains and can therefore be dissected by standard statistical methods. The QTLs for these traits impressively show the real interactions between the genes, which regulate the quantitative values of these parameters in the mixed allelic environment of RI strains.

As initially stated, QTL mapping is based on a statistical method that is used to determine the odds between diverse phenotypes and genotypes. If a specific allelic variation is associated with several up- or downregulated measured values, the same genomic location of the allelic variants will always appear as QTL for these regulated values. Hence, there is a bias in the detection of regulatory elements that are responsible for several related parameters as also shown in our data for the QTLs for lipid metabolism parameters such as cholesterol and high-density lipoproteins (Fig. 3). This behavior lies in the nature of the statistical mapping approach and can also be seen in the more recent expression QTL (eQTL) mapping, a variant of QTL mapping in which tissue-specific gene expression data are mapped onto a usually dense genetic map (9). Physiological QTLs combined with eQTLs—not utilized for this RI resource yet—would dramatically increase the power of this resource to the level of candidate gene detection.

Finally, it should be mentioned that these RI strains and all data on them are freely available at **http://www.anim.med.kyoto-u.ac.jp/nbr**. They have already been used by and can be distributed to interested researchers worldwide. Additional results obtained from this unique and largest available RI rat strain set will be forthcoming in the future. QTLs from this resource will be deposited into proficient QTL databases like the RGD database (19) and will not only improve our knowledge on rat physiology but also support progress in biomedical research across a range of species through comparative research approaches.

ACKNOWLEDGMENTS

This work was supported by the National Bio Resource Project for the Rat in Japan, which is part of the "Research Revolution 2002" (RR2002) initiative of the Japanese Ministry of Education, Culture, Sports, Science and Technology.

GRANTS

This work was also supported in part by Grants-in-aid for Scientific Research from the Japan Society for the Promotion of Science (18300141 to T. Kuramoto and 16200029 to T. Serikawa) and a Grant-in-aid for Cancer Research from the Ministry of Health, Labour and Welfare.

REFERENCES

1. **Adams N, Oldham TD, Briscoe JT, Hannah JA, Blizard DA.** Ethanol preference in Maudsley and RXNRA recombinant inbred strains of rats. *Alcohol* 24: 25–34, 2001.
2. **Aitman TJ, Glazier AM, Wallace CA, Cooper LD, Norsworthy PJ, Wahid FN, Al-Majali KM, Trembling PM, Mann CJ, Shoulders CC, Graf D, St Lezin E, Kurtz TW, Kren V, Pravenec M, Ibrahimi A, Abumrad NA, Stanton LW, Scott J.** Identification of Cd36 (Fat) as an insulin-resistance gene causing defective fatty acid and glucose metabolism in hypertensive rats. *Nat Genet* 21: 76–83, 1999.
3. **Atlas SA, Taylor BA, Diwan BA, Nebert DW.** Inducible monooxygenase activities and 3-methyl-cholanthrene-initiated tumorigenesis in mouse recombinant inbred sublines. *Genetics* 83: 537–550, 1976.
4. **Bailey DW.** Recombinant-inbred strains. An aid to finding identity, linkage, and function of histocompatibility and other genes. *Transplantation* 11: 325–327, 1971.
5. **Deschepper CF, Masciotra S, Zahabi A, Boutin-Ganache I, Picard S, Reudelhuber TL.** Functional alterations of the Nppa promoter are linked to cardiac ventricular hypertrophy in WKY/WKHA rat crosses. *Circ Res* 88: 223–228, 2001.
6. **Gibbs RA, Weinstock GM, Metzker ML, Muzny DM, Sodergren EJ, Scherer S, Scott G, Steffen D, Collins F.** Genome sequence of the Brown Norway rat yields insights into mammalian evolution. *Nature* 428: 493–521, 2004.
7. **Harshfield GA, Simmel EC.** Development of individual differences of cardiovascular regulation in the Bailey recombinant inbred mice. *Behav Genet* 9: 495–504, 1979.
8. **Hedrich H.** Recombinant inbred strains. In: *Genetic Monitoring of Inbred Strains of Rats*, edited by Hedrich HJ. Stuttgart, Germany: Gustav Fischer, 1990, p. 484–494.
9. **Hubner N, Wallace CA, Zimdahl H, Petretto E, Schulz H, Maciver F, Mueller M, Hummel O, Monti J, Zidek V, Musilova A, Kren V, Causton H, Game L, Born G, Schmidt S, Muller A, Cook SA, Kurtz TW, Whittaker J, Pravenec M, Aitman TJ.** Integrated transcriptional profiling and linkage analysis for identification of genes underlying disease. *Nat Genet* 37: 243–253, 2005.
11. **Lander E, Kruglyak L.** Genetic dissection of complex traits: guidelines for interpreting and reporting linkage results. *Nat Genet* 11: 241–247, 1995.
12. **Manly KF, Cudmore RH Jr, Meer JM.** Map Manager QTX, cross-platform software for genetic mapping. *Mamm Genome* 12: 930–932, 2001.
13. **Mashimo T, Voigt B, Kuramoto T, Serikawa T.** Rat Phenome Project: the untapped potential of existing rat strains. *J Appl Physiol* 98: 371–379, 2005.
14. **McKusick-Nathans Institute for Genetic Medicine, Johns Hopkins University and National Center for Biotechnology Information, National Library of Medicine.** *Online Mendelian Inheritance in Man (OMIM).* http://www.ncbi.nlm.nih.gov/omim/, March 12, 2007.
15. **Merryman CF, Maurer PH, Bailey DW.** Genetic control of immune response in mice to a glutamic acid, lysine, phenylalanine copolymer. 3. Use of recombinant inbred strains of mice to establish association of immune response genes with H-2 genotype. *J Immunol* 108: 937–940, 1972.
16. **Mouse Genome Informatics Web Site.** *Mouse Genome Database* (MGD). Jackson Laboratory, 2007.
17. **Page RD.** TreeView: an application to display phylogenetic trees on personal computers. *Comput Appl Biosci* 12: 357–358, 1996.
18. **Pravenec M.** Recombinant inbred strains—a model for the study of spontaneous hypertension in rats. *Cesk Fysiol* 35: 271–274, 1986.

19. **Rat Genome Database.** *R QTL Browser*. Medical College of Wisconsin, 2007.
20. **Shisa H, Lu L, Katoh H, Kawarai A, Tanuma J, Matsushima Y, Hiai H.** The LEXF: a new set of rat recombinant inbred strains between LE/Stm and F344. *Mamm Genome* 8: 324–327, 1997.
21. **STAR Consortium.** *Rat SNP analysis*. EURATools, 2007.
22. **Swofford D.** *PAUP: Phylogenetic Analysis Using Parsimony* (version 40b10). http://paup.csit.fsu.edu/, 2007.
23. **Tachibana M, Lu L, Hiai H, Tamura A, Matsushima Y, Shisa H.** Quantitative trait loci determining weight reduction of testes and pituitary by diethylstilbestrol in LEXF and FXLE recombinant inbred strain rats. *Exp Anim* 55: 91–95, 2006.
24. **Valdar W, Flint J, Mott R.** Simulating the collaborative cross: power of quantitative trait loci detection and mapping resolution in large sets of recombinant inbred strains of mice. *Genetics* 172: 1783–1797, 2006.
25. **Watson J, Riblet R, Taylor BA.** The response of recombinant inbred strains of mice to bacterial lipopolysaccharides. *J Immunol* 118: 2088–2093, 1977.

Exp. Anim. 58(1), 1–10, 2009

Characterization of the Kyoto Circling (KCI) Rat Carrying a Spontaneous Nonsense Mutation in the Protocadherin 15 (*Pcdh15*) Gene

Kuniko NAOI[1,4], Takashi KURAMOTO[1], Yuki KUWAMURA[2], Hiroshi GOHMA[1], Mitsuru KUWAMURA[3], and Tadao SERIKAWA[1]

[1]*Institute of Laboratory Animals, Graduate School of Medicine, Kyoto University, Yoshidakonoe-cho, Sakyo-ku, Kyoto 606-8501,* [2]*Osaka Pathology Center, Drug Safety Research Laboratories, Shin Nippon Biomedical Laboratories, LTD., 2–1–1 Fushimi-machi, Chuo-ku, Osaka 541-0044,* [3]*Laboratory of Veterinary Pathology, Osaka Prefecture University, 1–1 Gakuen-cho, Naka-ku, Sakai, Osaka 599-8531, and* [4]*Present address; Department of Medical Therapeutics, Molecular Therapeutics, Gifu Pharmaceutical University, 5–6–1 Mitahora-higashi, Gifu 502-8585, Japan*

Abstract: Protocadherin-15 (*Pcdh15*) plays important roles in the morphogenesis and cohesion of stereocilia bundles and in the maintenance of retinal photoreceptor cells. In humans, mutations in *PCDH15* cause Usher syndrome type 1F (USH1F) and non-syndromic deafness DFNB23. In mice, repertories of *Pcdh15* mutant alleles have been described as Ames waltzer mutations. For further understanding of *Pcdh15* function in vivo and to develop better clinical treatment for the disabling symptoms of USH1F and DFNB23 patients, animal models suitable for clinical as well as pharmacological studies are required. Here we report the characterization of a *Pcdh15* mutant allele, Kyoto circling, (*Pcdh15*^{kci}) in the rat. Rats homozygous for *Pcdh15*^{kci} display circling and abnormal swimming behaviors along with the lack of an auditory-evoked brainstem response at the highest intensities of acoustic stimulation. Positional cloning analysis revealed a nonsense mutation (c. 2911C>T, p. Arg971X) in the *Pcdh15* gene, which is predicted to result in the truncation of the PCDH15 protein at the 9th domain of cytoplasmic cadherin domains. Histological study revealed severe defects in cochlear hair cell stereocilia, collapse of the organ of Corti, and marked reduction of ganglion cells in adult *Pcdh15*^{kci} mutants. Severe reduction of sensory hair cells was also found in the saccular macula. Since the rat is more advantageous for clinical and pharmacological studies than the mouse, the KCI rat strain may be a better disease model for *Pcdh15*-deficit USH1F and DFNB23.

Key words: deafness, disease model, protocadherin 15, rat, USH1F

Introduction

Genetic analyses of congenital deafness in mice and rats and hereditary neurosensory disorders in humans largely serve to identify the genes responsible for hearing impairments [1, 16]. Genetic analysis of mouse Ames waltzer (*av*) mutation, which causes deafness and vestibular dysfunction associated with degeneration of

(Received 7 May 2008 / Accepted 22 July 2008)

Address corresponding: T. Serikawa, Institute of Laboratory Animals, Graduate School of Medicine, Kyoto University, Yoshidakonoe-cho, Sakyo-ku, Kyoto 606-8501, Japan

the inner ear neuroepithelia, identified protocadherin 15 (*Pcdh15*) as the gene responsible for hearing impairment [5]. Several different alleles have been identified in the *av* locus and include av^{J}, av^{2J}, av^{3J}, av^{6J}, av^{Tg} ($av^{TgN2742Rpw}$), av^{Jfb}, and av^{5J} (av^{nmf19}) [4, 5, 8, 17, 18]. Extensive analyses of these *av* mutants show that mutation in *Pcdh15* affects hair bundle morphogenesis and polarity [8, 12, 17] and mechanotransduction [7]. A detailed study on the localization and function of PCDH15 in hair cells by Senften *et al.* strongly supports the role of *Pcdh15* in bundle morphogenesis and polarity [14]. More recently, Kazmierczak *et al.* have shown by immunohistochemical studies using rodent hair cells and biochemical experiments that PCDH15 interacts with cadherin 23 to form tip-link filaments that connect the stereocilia and are thought to gate the mechanoelectrical transduction channel [10].

In humans, missense mutations of the *PCDH15* gene cause non-syndromic deafness, DFNB23, recessive prelingual hearing loss with normal vestibular responses and electroretinogram [3]. Meanwhile, nonsense mutations of the *PCDH15* cause Usher syndrome type 1F (USH1F), a recessive disorder characterized by congenital profound hearing loss, vestibular problems, and delayed retinitis pigmentosa [2, 6]. The prevalence of USH1F in USH1 patients varies among the cohort, but it is a relatively common subtype of USH1. To treat the deafness of USH1F patients, cochlear implantation is widely used. Recently, an aminoglycoside-dependent therapeutic approach has been attempted *in vitro* as a novel and definitive treatment of USH1F [13]. Whatever therapeutic approaches for USH1F and DFNB23 are chosen, it is currently necessary to validate them in an animal model that mimics the mutant phenotype of human diseases. The laboratory rat (*Rattus norvegicus*) provides important mammalian models for various human diseases. Due to its suitable body size and great adaptability, the rat serves as an animal model especially in neurological, behavioral, surgical and pharmacological studies. An experimental system with the rat model for USH1F and DFNB23 would be advantageous, especially when the causative gene of the rat model is identified as a mutation of *Pcdh15*.

Rats showing abnormal behaviors characterized by constant circling movements were found in the F_3 generation of Crl:CD(SD) rats purchased from Charles River Laboratory Japan (Kanagawa, Japan) in 2003. Preliminary genetic analysis showed that these abnormal traits were inherited in an autosomal recessive manner. Although inbreeding has not been fully completed (F18), we called the rats Kyoto Circling (KCI) and named the causative gene *kci*.

In this report, we describe the identification of the *kci* as a nonsense mutation of the *Pcdh15* gene, and the histopathological characteristics of the KCI rat.

Materials and Methods

Animals

KCI rats were provided by the National Bio Resource Project for the Rat in Japan and kept in our animal facility for all experiments in this study. BN/SsNSlc rats were purchased from Japan SLC, Inc. (Shizuoka, Japan). KCI rats were bred by a brother-sister mating of *kci/+* heterozygous females with *kci/kci* homozygous males. Animal care and experimental procedures were approved by the Animal Research Committee, Kyoto University and were conducted according to the Regulation on Animal Experimentation at Kyoto University.

Auditory brainstem response measurement

Auditory brainstem response (ABR) measurements were performed in three individuals each for *kci/+* heterozygous and *kci/kci* homozygous rats at 9 weeks of age. The following experiments were performed using animals anesthetized with ketamine (80 mg/kg, i.p.) and xylazine (8 mg/kg, i.p.). Stainless steel needle electrodes were inserted subcutaneously into the vertex (indifferent), one side (active), and the other side (ground) of the retroauricular region. The ABR was obtained by averaging 1,000 evoked responses to click stimuli at intensities of 43, 52, 63, 72, 81, and 90 dB peak equivalent sound pressure levels (peSPL) with 50-ms intervals generated by an acoustic stimulator (MEB-5504, Nihon Koden, Tokyo, Japan). Clicks were delivered through an inner ear type earphone facing the meatus acusticus externus. ABR thresholds were detemined for each stimulus frequency by identifying the lowest intensity producing a reproducible ABR pattern on the computer screen (at least two consistent peaks).

Table 1. Primers used for amplifying rat *Pcdh15* cDNA

Primer name	Forward (5'>3')	Reverse (5'>3')	Position*
c*Pcdh15*.1	ATGTCCCCACAGTTT	CGTTGCCAGTCAACATGAGT	412–1066
c*Pcdh15*.2	CCAGAAGATCCGACATCCAA	CTGCAGTCAGCTGGATGACA	1009–2027
c*Pcdh15*.3	GTTTACACGGACATGAGTCC	GAACACGGGAGCGTTATCAT	1978–2577
c*Pcdh15*.4	GCCACTGTGAACATAGTGGT	GGAAACTGCACATCATCCAC	2527–3344
c*Pcdh15*.5	GTTTATGCTGAAGACGCAG	GCTATAGTCTTCTAGGGAG	3268–4338
c*Pcdh15*.6	GTTGTAGAGTCCATTGGTGC	CCACACCCTCTGGATCTTTT	4279–5145
c*Pcdh15*.7	GTTAAGAGTCAGTCCCTGAG	TTACAAGGACGTT	5095–6234

*Nucleotide positions of 5' and 3' ends of PCR products for rat *Pcdh15* cDNA (XM_001080000).

Genetic mapping

(BN/SsNSlc × KCI)F_1 rats were backcrossed to KCI to obtain N_2 rats. Homozygous *kcl/kci* animals were identified on the basis of the appearance of circling behavior and inability to swim at 3–4 weeks of age. A total of 259 N_2 progeny were produced in this study. Genomic DNA was prepared from tail biopsy using the automatic DNA purification system (PI-200, Kurabo, Japan). For the initial mapping of *kci*, we employed pooled-SSLP analysis [15]. DNA from 14 randomly selected rats of each genotype at the *kci* locus was standardized to 20 ng/μl and equal amounts of individual DNA were pooled with respect to each genotype. The *kcl/kci* and *kcl/+* DNA pools were genotyped for 61 microsatellite markers distributed among all autosomal chromosomes. The KCI rats used in the genetic study were homozygous for all of these markers. For the fine mapping of *kci*, all N_2 animals were genotyped.

RNA extraction and RT-PCR

Total RNA was extracted from the brain of 7-week-old animals with ISOGEN (Nippon Gene, Japan) according to the manufacturer's instructions and was stored in RNA Storage Solution (Ambion). Five micrograms of total RNA was used for first-strand cDNA synthesis with Superscript II reverse transcriptase (Invitrogen), and a 1-μl aliquot of 50 μl of reaction mixture was used as a template for PCR. Rat *Pcdh15* cDNAs were amplified with 7 sets of primers (Table 1). These PCR products overlapped each other and spanned the entire coding sequence of *Pcdh15*.

Sequencing

PCR products were treated with ExoSAP-IT (Amersham Biosciences) to digest single-strand DNAs and excess primers. Cycle sequencing was performed with the BigDye Terminator Ready Reaction Mix v3.1 according to the manufacturer's instructions (Applied Biosystems). PCR samples were purified with CENTRI-SEP spin columns and then loaded into an ABI PRISM 3100 genetic analyzer (Applied Biosystems).

Histopathology

We examined the inner ears of 4 *kcl/kci* homozygous mutant rats and 4 control (*kcl/+* heterozygous) rats at 16 weeks of age. Perfusion fixation through the left ventricle was conducted with Karnovsky solution (5% glutaraldehyde and 4% paraformaldehyde) under anesthesia. For light microscopy, the removed cochlea were fixed in 10% neutral-buffered formalin for 24 h and decalcified in ethylene diamine tetraacetic acid (EDTA). The specimens were then dehydrated in graded ethanol, embedded in paraffin and stained with hematoxylin and eosin (HE) or embedded in epoxy resin and stained with toluidine blue.

For scanning electron microscopy (SEM), the removed cochleae were immersed in 4% glutaraldehyde in 0.1 M phosphate buffer (pH 7.4) for 24 to 48 h. After dehydration and critical point drying under a dissecting microscope, the vestibule and membrane tectoria ductus cochlearis were removed. The blocks of tissues were covered with ionized gold and visualized under a scanning electron microscope (JSM-5200, JEOL, Tokyo, Japan). The surface view of the organ of Corti was analyzed.

For retina histology, eyes were removed from 4 *kcl/kci* homozygous mutant rats and 2 control rats at 16 weeks of age after anesthetic overdose followed by cervical

dislocation. Eyes were fixed overnight in Davidson's fixation solution, embedded in paraffin, and stained with HE.

Results

Mutant phenotype

Mutant offspring are identifiable at approximately 15 days of age by manifestation of twisting the neck toward the back when lifted by the tail. After weaning, mutant rats fail to show a startle response and display head tossing and bidirectional circling behavior. Circling behavior is observed as early as 14 days of age and persists throughout life. When the KCI rats were placed into a deep tank filled with warm water (35°C), they immediately began rotating along their long axis and sank. While underwater, the rats still rotated along their body length. The rats seldom resurfaced before they were rescued. These findings suggest that KCI rats might have lost their balance and have defects in the inner ear, which senses linear and angular acceleration.

Auditory brainstem response

In addition to this balance disorder, the KCI rats showed no response to sounds such as knocking and clapping. To test the auditory organ function, we measured ABR in KCI homozygous (*kci/kci*) rats and their normal littermates (*kci/+*). In *kci/+* heterozygotes, ABRs composed of I, II, III, IV, and V peaks were observed at all of the intensities examined (Fig. 1A), but no *kci/kci* homozygotes exhibited ABR up to the maximum level of acoustic stimulation (Fig. 1B), indicating that the KCI rats were completely deaf.

Genetic analysis

Pooled-SSLP analysis showed a linkage relationship between *D20Rat4* and the *kci* locus. A distinct reduction of the BN allelic fragment of the *D20Rat4* was seen in the *kci/kci* pool relative to both the F_1 hybrid and the *kci/+* pools. A genetic linkage study of 259 (BN/SsNSlc × KCI)F_1 × KCI backcross progeny using 3 additional markers on Chr 20 narrowed down *kci* to a 2.3-cM interval between *Rab36* and *D20Rat75* (Fig. 2A). Within this interval, three genes, *Rab36* (member RAS oncogene family), *Gnaz* (guanine nucleotide binding protein, alpha z subunit), and *Pcdh15* (protocadherin 15), and three predicted transcripts (RGD1561987, LOC502417 and RGD1563351) have been mapped, and these genes were considered as candidates for *kci* (Fig. 2B). *Pcdh15* was considered to be the strongest candidate among them, because mutations of this gene are responsible for deafness in humans and mice.

Although the expression level and size of the *Pcdh15* transcript are not altered in KCI rats, sequencing analyses of the entire coding region revealed the substitution of a cytosine to a tymidine residue at nucleotide position 2911 from the start of the coding region (c. 2911 C>T) (Fig. 2C), which was verified by PCR-RFLP analysis (Fig. 2D). This substitution introduces a stop codon at the 971st amino acid of the PCDH15 protein of the KCI rat (p. Arg971X). In the presence of the premature stop codon, the PCDH15 protein expressed in the *kci* allele would be truncated after the ninth extracellular cadherin domain (Fig. 2E). The *kci* nonsense mutation was completely associated with mutant phenotypes in 259 backcross progeny and not shared among 62 Crj:CD(SD) rats (data not shown). These findings suggest that the nonsense mutation of *Pcdh15* is responsible for the *kci* mutant phenotype.

Histopathological analysis

As illustrated in Fig. 3, stereocilia of both inner and outer hair cells of affected mutants were severely disorganized compared to those of control animals in which stereocilia were of normal configuration. The normal "V"-shaped arrangement of stereocilia was completely disrupted in all three rows of outer hair cells (Fig. 3). Stereocilia were misoriented and thickly fused. Inner hair cell stereocilia also showed a disorderly arrangement compared to controls (Fig. 3).

In the cochlea of *kci/kci* rats, severe to total loss of inner and outer hair cells was found (Fig. 4). The organ of Corti was collapsed into a poorly differentiated mass of cells in which the normal arrangement of fluid spaces was not noticeable. The number of cochlear nerve fibers in the osseous spiral lamina was dramatically reduced (Figs. 4A and 4B). Despite the severe degeneration of the organ of Corti in affected animals, the configuration of the cochlear duct remained normal. Reissner's membrane was in its normal position and no abnormalities of

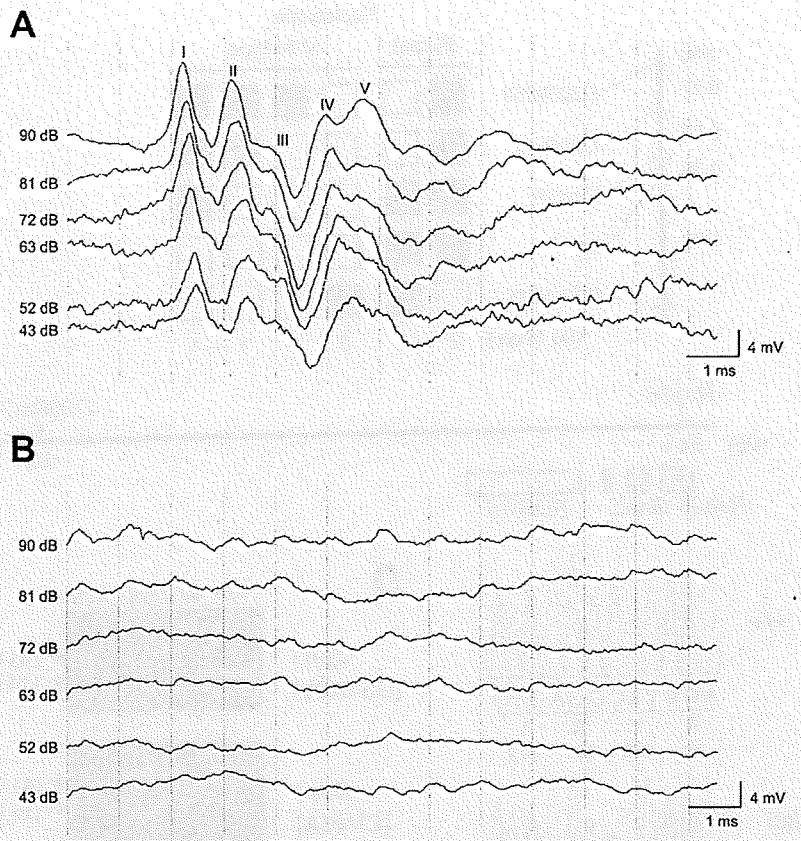

Fig. 1. Representative ABR waveforms of *kci*/+ heterozygous (A) and *kci*/*kci* homozygous (B) rats at 9 weeks of age. Five major peaks were detected for *kci*/+ heterozygous rats at the various intensities tested (43–90 dB). No peaks were obtained for *kci*/*kci* homozygous rats.

the stria vascularis were observed by light microscopy. The number of spiral ganglion cells was also reduced (Figs. 4C and 4D).

In the saccula macula of *kci*/*kci* rats, the number of sensory hair cells was severely reduced compared to control rats, although that of supporting cells seemed to be normal. The remaining hair cells appeared to be degenerated and the otolithic membrane was very severely damaged (Figs. 4E and 4F).

In the retina, no anatomical defects were noted in any *kci*/*kci* homozygous or heterozygous rats (Fig. 5). Retinas from all animals included all normal retinal layers, and no abnormalities were noted in the cellular structure as examined at the light microscopic level.

Discussion

The behavior of rats homozygous for the *kci* mutation is very similar to those described previously in mouse *Pcdh15*-mutant alleles [4, 5, 8, 17, 18]. The mutation in the *kci* allele is a nonsense mutation (c. 2911 C>T, p. Arg971X) and is predicted to result in truncated PCDH15 protein at the 9th domain of extracellular cadherin domains. This substitution was completely correlated with behavioral abnormalities in backcross progeny and was not shared by the outbred colony from which founders of KCI were discovered. Based on genotype-phenotype correlation and a significantly similar phenotype with *Pcdh15*-mutant Ames waltzer mice, we concluded that *Pcdh15* was the gene responsible for the mutant phenotype of the KCI rat. The *kci* is designated $Pcdh15^{kci}$.

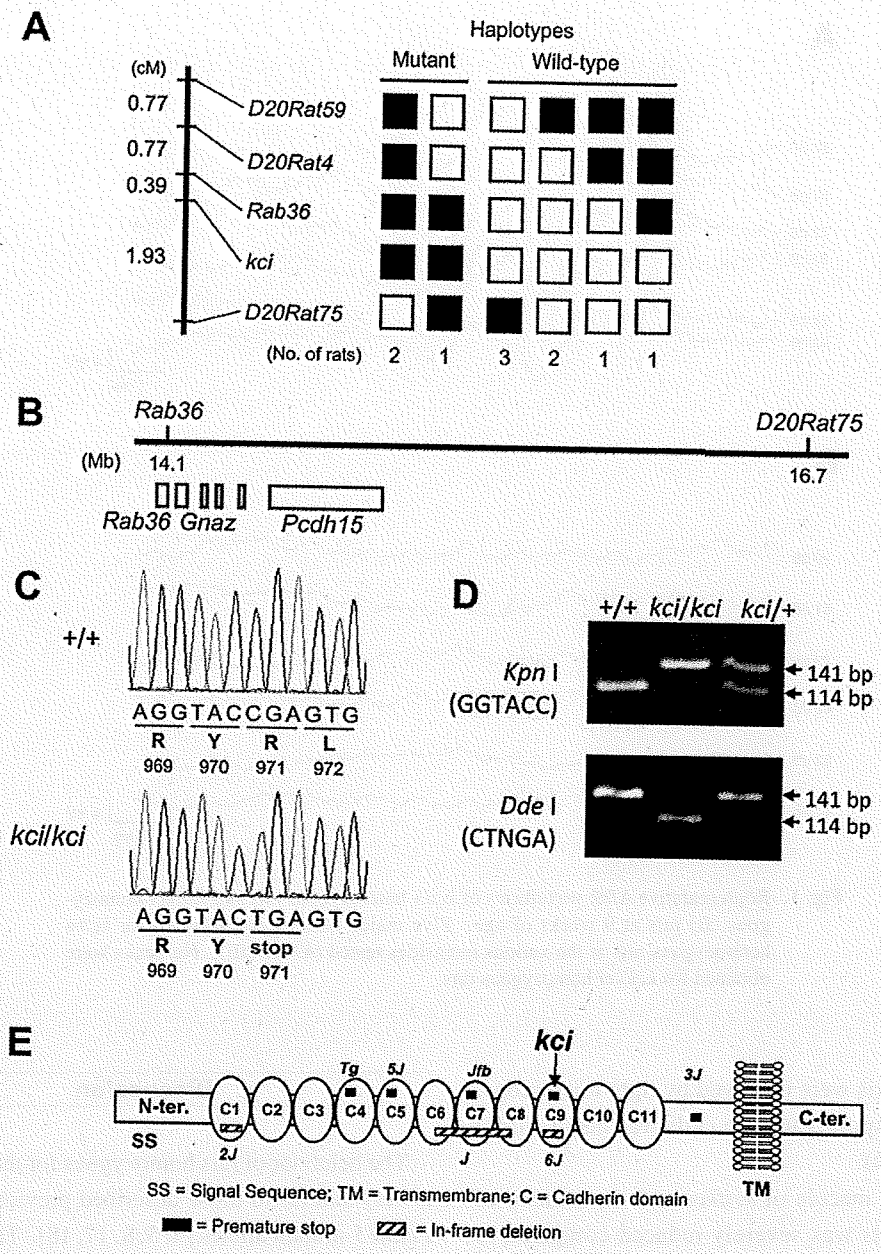

Fig. 2. Identification of the rat *kci* mutation. (A) Genetic linkage map around the *kci* locus (left). Distribution of haplotypes observed among 10 progeny carrying a recombinant chromosome between *D20Rat59* and *D20Rat75*. Black boxes, homozygote for the *kci* allele. White boxes, heterozygote for the *kci* and BN alleles. (B) The *kci* locus was physically localized to the 2.6-Mb region defined with *Rab36* and *D20Rat75*. Within the *kci* locus, three genes (white boxes) and three predicted transcripts (gray boxes) have been mapped. (C) Sequence analysis of *Pchd15* cDNA from wild-type and *kci/kci* rats. In the *kci/kci* rat, a nucleotide conversion C to T (red) occurred at the position of nucleotide 2911 of the rat *Pchd15* cDNA. The *kci* mutation generates a premature termination at codon 971 of the putative PCDH15 protein. Due to the *kci* mutation, a *Kpn*I site (GGTACC) is lost and a *Dde*I site (CTNAG) is generated. (D) Molecular diagnosis for the *kci* mutation. PCR products amplified with a pair of primers, rPcdh15kci-F (5'- GGGTTGCCAGCAAGTCGG -3') and rPcdh15kci-R (5'- CTTAAAAATTGTTGTAGGCTC -3'), were subjected to restriction digestion with *Kpn*I (upper) or *Dde*I (lower). A 141-bp PCR product from the wild-type allele was digested with *Kpn*I to 114-bp and 27-bp fragments, but not with *Dde*I, while a 141-bp PCR product from the *kci* allele was digested with *Dde*I to 114-bp and 27-bp fragments, but not with *Kpn*I. Note that the 27-bp fragment was too small to be seen. The CD(SD) rat was used as a control (+/+). (E) Schematic representation of PCDH15 indicating cadherin repeats (C1-C11), transmembrane domain (TM), and cytoplasmic domain. In the KCI rat, the protein is prematurely truncated and lacks the last two cadherin domains, transmembrane and cytoplasmic domains.

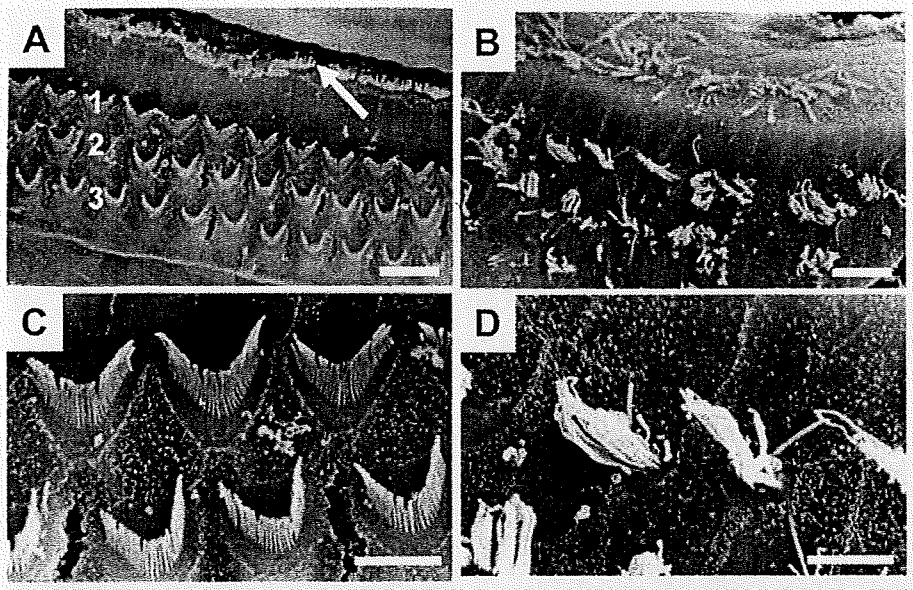

Fig. 3. Scanning electron micrograph of the organ of Corti from control (*kcil*+) (A, C) and homozygous (*kcil/kci*) (B, D) rats at 16 weeks of age. The single row of inner hair cells is indicated by an arrow and the three rows of outer hair cells (A) are labeled 1, 2, and 3. Stereocilia in the control show a normal configuration. In the *kcil/kci* rat, stereocilia of both inner and outer hair cells are severely disorganized. Most outer hair cells lose their stereocilia and the remaining stereocilia are shortened, fused, and disorientated. Bar=10 μm (A, B). Bar=5 μm (C, D)

The *Pcdh15*^{kci} allele is a functional null, because the mutation introduces a stop codon, and it is included in the repertoire of rodent *Pcdh15* mutant alleles. Mature KCI rats show constant circling behavior and histological defects in both cochlear and vestibular hair cells, which are comparable with those observed in mouse *Pcdh15*-null alleles such as *av*^{Tg}, *av*^{5J}, or *av*^{Jfb} [4, 8, 17]. Behavioral and histological findings of KCI rats indicate that PCDH15 is also indispensable in stereocilia bundle morphogenesis in rats. In addition to analyses of different alleles of *av*, further extensive analyses of KCI rats will allow us to understand the function of *Pcdh15* in inner hair cell development and the cause of inner ear disorders in USH1F and DFNB23 patients.

As an animal model for USH1F and DFNB23, KCI rats have great advantages over the *av* null-mutant mice. Since the rat has suitable body size for artificial manipulation, the KCI rat could serve as a better disease model in the development of novel clinical treatments for USH1F and DFNB23. In the rat, ample data on physiology and pharmacology have been accumulated. Thus, the KCI rat could also serve as a better disease model in the development of new drugs for USH1F and DFNB23.

Patients with USH1F suffer from progressive retinitis pigmentosa, in addition to profound congenital hearing loss and vestibular deficits [11]. Although cochlear implantation can recover auditory perception, there are no clinical treatments for recovery of visual perception, thus, animal models for retinitis pigmentosa in USH1F patients have been greatly anticipated. Although PCDH15 protein is known to be expressed in the rodent retina [9], we could not detect any evidence of retinal degeneration or disorganization in the KCI mutant rat. To identify functional abnormalities of the retina in the KCI rat, further analyses, such as electroretinograms and electron microscopic observations, will be necessary. In *av* mice, it has been reported that two nonsense *av* mutations, *Pcdh15*^{av5J} and *Pcdh15*^{avJfb}, show significantly attenuated but stable electroretinograms in the absence of histopathology of the retina [9].

In summary, we established the KCI rat strain and identified the causative gene of the KCI mutant phenotype as the Arg971X mutation of the *Pcdh15* gene. The

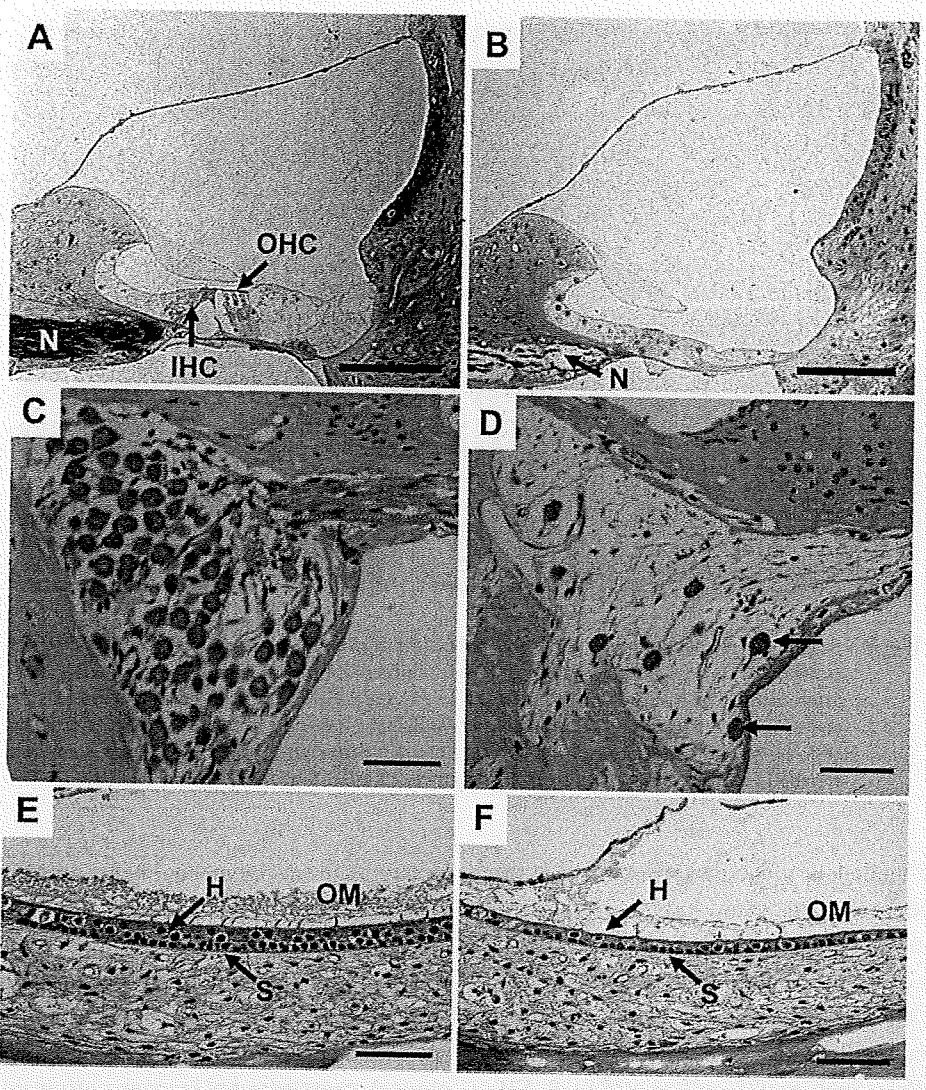

Fig. 4. Histology of cochlear (A, B), spiral ganglion (C, D), and saccular macula (E, F) in control (A, C, E) and *kci/kci* rats (B, D, F) at 16 weeks of age. (A) The organ of Corti from a control animal with normal inner hair cells (IHC) and outer hair cells (OHC) and intraepithelial fluid spaces. The osseous spiral lamina is filled with myelinated nerve fibers (N). (B) The collapsed organ of Corti and the degeneration of inner and outer hair cells in the *kci/kci*. There is also a dramatic reduction in the number of myelinated nerve fibers (arrow) in the osseous spiral lamina. (C) Cross sections of the spiral ganglion from a control cochlear. (D) The spiral ganglion (arrows) from the *kci/kci* rat showing reduced numbers of ganglion cells in an affected animal at 16 weeks of age. (D) The saccular macula from a control animal with normal sensory hair (H) and supporting (S) cells. (E) Cross section of the saccular macula demonstrating a marked decrease in the number of hair cells (H) in an affected animal. The otolithic membrane (OM) was also severely damaged. The supporting cells (S) appear normal. The specimens were embedded in epoxy resin and stained with toluidine blue (A, B) or embedded in paraffin and stained with hematoxylin and eosin (C–F). Bar=100 μm (A, B). Bar=50 μm (C–F).